JOURNAL OF GEOPHYSICAL RESEARCH, VOL. 105, NO. A11, PAGES 25,143–25,154, NOVEMBER 1, 2000

The interplanetary shock of September 24, 1998: Arrival at Earth

C. T. Russell,[1] Y. L. Wang,[1] J. Raeder,[1] R. L. Tokar,[2] C. W. Smith,[3] K. W. Ogilvie,[4] A. J. Lazarus,[5] R. P. Lepping,[4] A. Szabo,[4] H. Kawano,[6] T. Mukai,[7] S. Savin,[8] Y. I. Yermolaev,[8] X.-Y. Zhou,[9,10] and B. T. Tsurutani[9]

Abstract. At close to 2345 UT on September 24, 1998, the magnetosphere was suddenly compressed by the passage of an interplanetary shock. In order to properly interpret the magnetospheric events triggered by the arrival of this shock, we calculate the orientation of the shock, its velocity, and its estimated time of arrival at the nose of the magnetosphere. Our best fit shock normal has an orientation of (-0.981 -0.157 -0.112) in solar ecliptic coordinates, a speed of 769 km/s, and an arrival time of 2344:19 at the magnetopause at 10 R_E. Since measurements of the solar wind and interplanetary magnetic field are available from multiple spacecraft, we can compare several different techniques of shock-normal determination. Of the single spacecraft techniques the magnetic coplanarity solution is most accurate and the mixed mode solution is of lesser accuracy. Uncertainty in the timing and location of the IMP 8 spacecraft limits the accuracy of solutions using the time of arrival at the position of IMP 8.

1. Introduction

The flotilla of International Solar Terrestrial Physics (ISTP) spacecraft [e.g., *Russell,* 1997] hold the promise of being able to address many of the issues surrounding the global dynamics of the magnetosphere. In mid 1998 three spacecraft, ACE, Wind, and IMP 8, routinely monitored the solar wind. All were relatively close to the Earth-Sun line in contrast to the cross-flow distance of the earlier ISEE 3 spacecraft, the designated L1 solar wind monitor during the International Magnetospheric Study (IMS) period [e.g., *Russell and Southwood,* 1982]. These spacecraft were joined by the Interball Tail Probe, Geotail, and Polar that were designed to study the tail, magnetosheath, near-Earth solar wind, outer magnetosphere, and aurora. In addition there were a host of spacecraft in the magnetosphere such as NOAA's GOES 8 and 10, and Los Alamos surveillance spacecraft in synchronous orbit, and FAST and DMSP spacecraft in low-Earth, polar orbit. An important issue, when a strong shock arrives, as it did late on September 24, 1998, is to determine its orientation and speed so that its precise time and location of arrival can be ascertained. Modern MHD simulations [e.g., *Raeder,* 1999] can be then used to predict how the disturbance propagates through the magnetosphere and its predicted and observed affects can be intercompared. Other studies such as those of the propagation of the sudden impulse, and the brightening of the aurora due to the pressure change also benefit from knowing the arrival time and shock orientation. It is the objective of this paper to use all the available solar wind and interplanetary data on this day to determine accurately the shock orientation, speed, intensity, and time of arrival at the Earth. In fact, we have so much data on the arrival of this shock that we can overdetermine the solution and use that overdetermination to examine the accuracy of the various techniques used to determine shock normals.

The importance of making an accurate determination of the parameters associated with the arrival of this shock is presaged by the number of studies of the magnetospheric effects of this shock that have appeared or are in work. The arrival of the shock and its affect on the magnetic field at Polar, high over the polar cap, at GOES 10 on the dayside, and GOES 8 past dusk have been discussed by *Russell et al.* [1999]. The polar cap ion flows induced by the passage of the shock have been discussed by *Moore et al.* [1999] and of the outflows at FAST by *Strangeway et al.* [2000]. The depletion and refilling of the plasmasphere has been examined by *Chi et al.* [2000]. Studies are in progress of the X-ray observations of the auroral oval of the field-aligned current system deduced from the assimilated mapping of ionospheric electrodynamics (AMIE) inversion of ground-based magnetometer networks of the propagation of the sudden impulse through the magnetosphere. The principal objective of this paper is to derive an accurate shock normal direction and speed and the shock arrival time to enable studies of the propagation of the shock through the magnetosphere. The wealth of shock observations on this day enables us to intercompare techniques and observations at different sites. These data enable us to test methods and assumptions about the shock such as its time stationarity and planarity.

In the sections that follow we review first the locations of the spacecraft in the solar wind and their observations. Then we discuss the techniques used to determine shock normals and shock speeds. Next, we apply these techniques to the

[1]Institute of Geophysics and Planetary Physics, University of California Los Angeles.
[2]Los Alamos National Laboratory, Los Alamos, New Mexico.
[3]Bartol Research Institute, University of Delaware, Newark.
[4]NASA/Goddard Space Flight Center, Greenbelt, Maryland.
[5]Center for Space Research, Massachussetts Institute of Technology, Cambridge.
[6]Dept. Earth and Planetary Sciences, Kyushu University, Higashu-Ku, Fukuoka, Japan.
[7]Institute of Space and Astronautical Science, 311 Yoshinodai Sagamihara, Kanagawa, Japan.
[8]Space Research Institute, Moscow, Russia.
[9]Jet Propulsion Laboratory, Pasadena, California.
[10] Institute of Geophysics, Chinese Academy of Sciences, Beijing, China.

Paper number 2000JA900070
0148-0227/00/2000JA900070$09.00

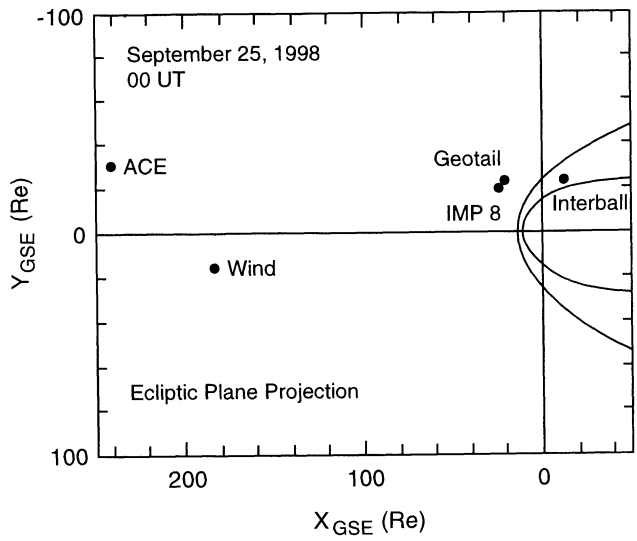

Figure 1. Ecliptic plane projection of the positions of the ACE, Wind, Geotail, IMP 8, and Interball spacecraft at 0000 UT on September 25, 1998, shortly after the arrival of the interplanetary shock.

observations on September 24, 1998, and determine the best fit orientation, speed, and arrival time. Finally, we discuss the reasons for the successes and failures of the various techniques and provide cautionary notes for the practitioner.

2. Shock Observations

On September 24, 1998, at 2313 UT a strong interplanetary shock crossed the ACE spacecraft at 241 R_E upstream of the Earth. At 2321 UT the shock reached the Wind spacecraft 184 R_E upstream of the Earth and later IMP 8 and Geotail in the near-Earth solar wind and the Interball Tail Probe in the magnetosheath. The location of these five spacecraft are shown in Figure 1 projected into the ecliptic plane. Figure 2 shows the orthogonal projection as seen from the Sun. This plot emphasizes the rather close spacing of the spacecraft orthogonal to the Sun-Earth line. The total width of this figure is 60 R_E compared with the 240 R_E distance of ACE from the Earth at this time. Thus the measurements made by these spacecraft all should be relevant to the plasma that intercepts the Earth's bow shock and magnetopause. On the other hand, this close spacing requires rather precise timing of the shock encounter if we wish to determine the orientation of the shock solely from its time of arrival at the four solar wind spacecraft as we can on this day. Figure 2 shows the locations of these spacecraft in GSM coordinates for the convenience of those studying the solar wind interaction with the magnetosphere. In this paper all calculations are performed in GSE coordinates because it is closer to an inertial system than GSM.

To determine the shock arrival at each spacecraft, we use the magnetic field because it is measured with the greatest cadence. Figure 3 shows the magnetic field measured by the ACE magnetometer at a rate of 3 times a second [*Smith et al.*, 1998]. The time given in Table 1 is the time when the magnetic field magnitude reached the halfway point between its upstream and

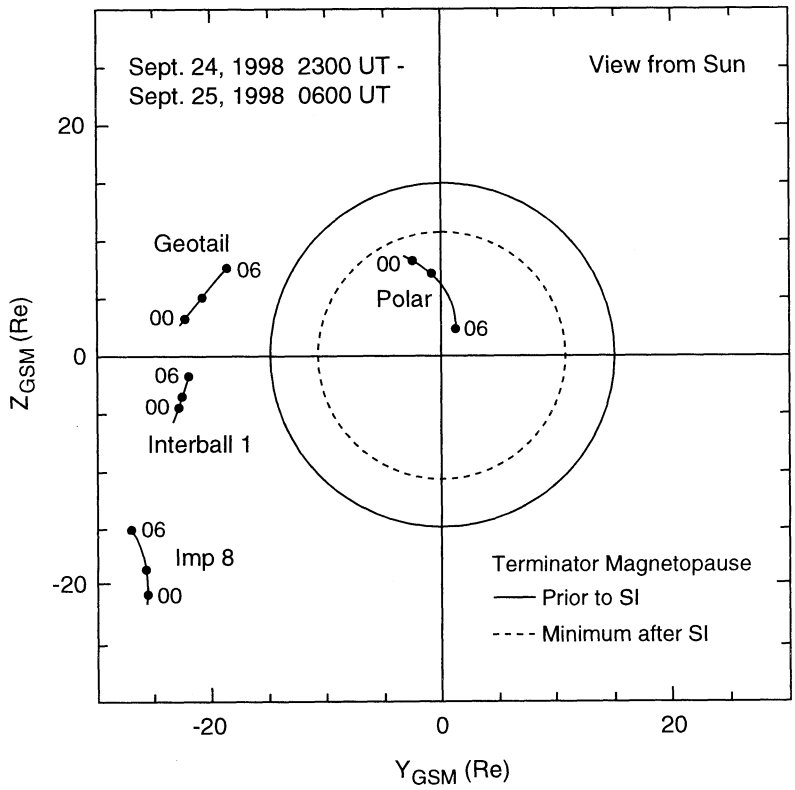

Figure 2. Projection of the orbits of ACE, Wind, Geotail, Interball, and IMP 8 on the phase perpendicular to the solar wind flow in GSM coordinates.

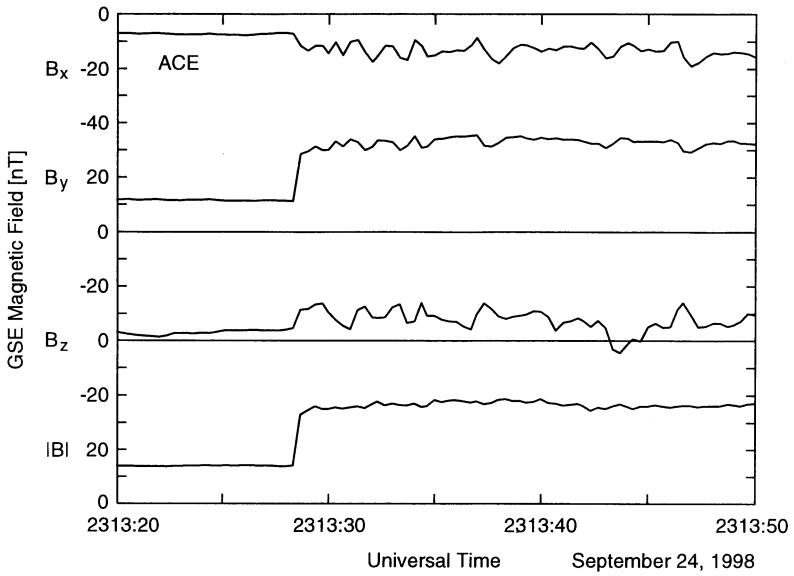

Figure 3. Magnetic field measured by ACE across the interplanetary shock in GSE coordinates.

downstream asymptotic values. The timing of the ACE samples is known to the nearest 330 ms in UT, and we can make the time of arrival estimate to about one half of a sample period or 160 ms here because of the sharpness of the profile.

Figure 4 shows the magnetic field measurements from the Wind spacecraft [*Lepping et al.,* 1995]. These data were obtained at a rate of 10.9 samples per second. Again the profile is sharp and we can determine the time halfway up the ramp to the nearest 50 ms.

Figure 5 shows the magnetic field measurements from the Geotail spacecraft [*Kokubun et al.,* 1994]. These data were obtained at a rate of 16 samples per second. As before, the profile is sharp and we can time the samples to the nearest 30 ms.

Presently, the IMP 8 magnetometer saturates when any component exceeds 36 nT. As the shock crossed IMP 8 the field did exceed this value. Nevertheless, we can still determine the shock encounter time with sufficient accuracy for our shock normal determination despite the saturation. We find that the shock front crossed IMP 8 at 2344:25 UT within ±1 s. The location of IMP 8 is presently not as well determined, and we might expect an error of up to 0.7 R_E in each of its coordinates. Unlike the other spacecraft in our study, no ranging information is now obtained from IMP 8. The locations of all four solar wind spacecraft and the magnetosheath spacecraft Interball and the times of arrival of the shock at each are given in Table 1.

Since we have the time of arrival of the shock at four spacecraft in the solar wind we can immediately invert the matrix of locations of three of the spacecraft referenced to the fourth spacecraft and multiply the inverted matrix times the corresponding time difference vector to get the speed and orientation of the shock [*Russell et al.,* 1983a]. (We do not use the Interball spacecraft here because it is in the magnetosheath.) Most importantly, we can use this matrix to estimate the accuracy we require for each of the difference vectors and travel time to achieve an accuracy of 1° in the direction of the normal. These accuracies are listed in Table 2. These numbers can then guide us to the accuracy that we need to achieve in timing the shock and locating the spacecraft. It might be thought that the 0.7 R_E uncertainty in the IMP 8 location would be the limiting factor, but as will become evident below, we found another unexpected source of inaccuracy in these data. One value in this table appears to be exceeded by a factor of 17. It is for this reason we do not quote the normal orientation and shock speed at this time.

Table 1. Location and Arrival Times of Shock.

Spacecraft	Time of Arrival, UT	GSE Location of Spacecraft		
		X, R_E	Y, R_E	Z, R_E
ACE	2313:28.5	241.40	-30.06	12.97
Wind	2320:37.5	183.64	14.70	-5.85
Geotail	2343:29.8	20.22	-22.45	-2.21
IMP 8	2344:24-26	24.24	-19.92	-26.10
Interball	2348:15	-11.46	-21.27	-9.70

The magnetometer data can be used more than just for timing the shock arrival. The changes in the vector components across the shock is determined by the orientation of the shock front and can be in turn used to determine this orientation. This allows the orientation of the shock to be determined locally rather than globally as in our four spacecraft solution that assumes that the front is planar and smooth over the volume occupied by the four spacecraft. In theory, the change in magnetic field should be measured nearly simultaneously at an upstream and downstream monitor as a particular parcel of magnetized plasma crosses one and then the other spacecraft. To approximate this coincident sampling, we attempt to measure the upstream and downstream values as close as possible to the shock ramp to minimize the possibility of a temporal change being mistaken for a spatial one. Because of their rapid cadence this can best be done with the magnetometers. Nevertheless, the interplanetary magnetic field is also more changeable than the solar wind parameters, thus possibly negating some of the advantage of the greater cadence.

Solar wind plasma measurements are obtained at a significantly lower cadence. In theory, these data could also be very useful for determining the shock orientation because the shock normal direction affects the change in the flow direction across the shock. Moreover, we can use the compression of the plasma across the shock together with the change in flow velocity to determine the speed of the shock. This is especially important in situations when there are fewer than four spacecraft in the solar wind monitoring the shock passage. However, the solar wind is a

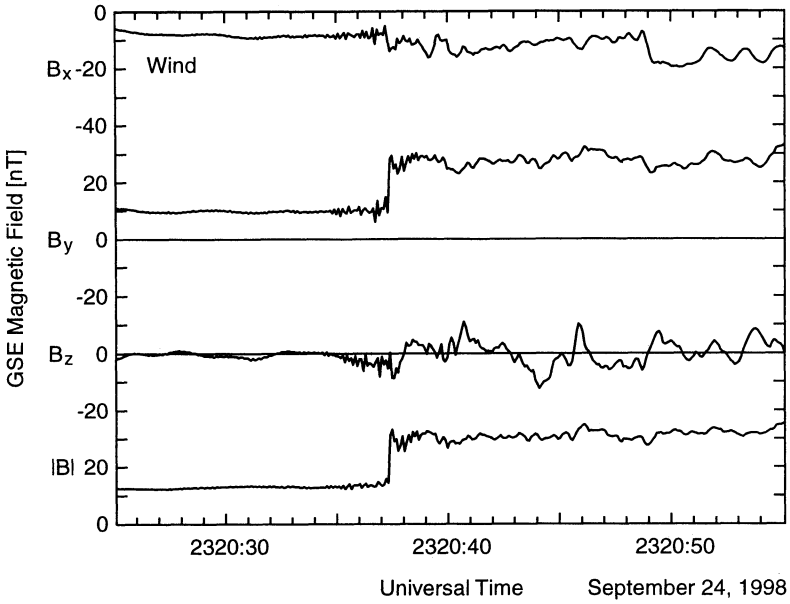

Figure 4. Magnetic field measured by Wind across the interplanetary shock in GSE coordinates.

multi-ion plasma, and most solar wind monitors do not have mass separation. At some ion temperatures and bulk velocities it is difficult to unambiguously determine the individual contributions to the measured flux, and this relative contribution may change as the shock crosses the spacecraft. Hence their accuracy is limited. Again the solar wind data provide a local measure of the shock normal and can in theory test the planar shock assumption. Thus we examine the plasma data across the shock front at each of its spacecraft for which data are available.

Figure 6 shows the arrival of the shock at ACE in the three components of the velocity and the solar wind densities [*McComas et al.*, 1998]. The speed jumps smoothly from about 440 km/s its usual speed to 650 km/s. Figures 7 and 8 show the equivalent data at Wind [*Ogilvie et al.*, 1995] and from the Geotail solar wind ion analyzer [*Mukai et al.*, 1994].

Finally, we note that the Interball Tail Probe was crossed by the shock at 2348:15 while it was in the magnetosheath and 11.46 R_E behind the dawn terminator. Figure 9 shows the magnetic field in GSE coordinates [*Klimov et al.*, 1997] and the Corall ion spectra from 0.03 to 25 keV [*Yermolaev et al.*, 1997]. The Interball spacecraft slowly rotates about the Sun line with a 2-min period, thus accounting for the periodic appearance of the ion spectra, but the shock onset can be seen clearly and accurately timed in both the ion spectra and the magnetic field.

This is an important fiducial marker because it gives a precise time of arrival at a point geospace that is well within the

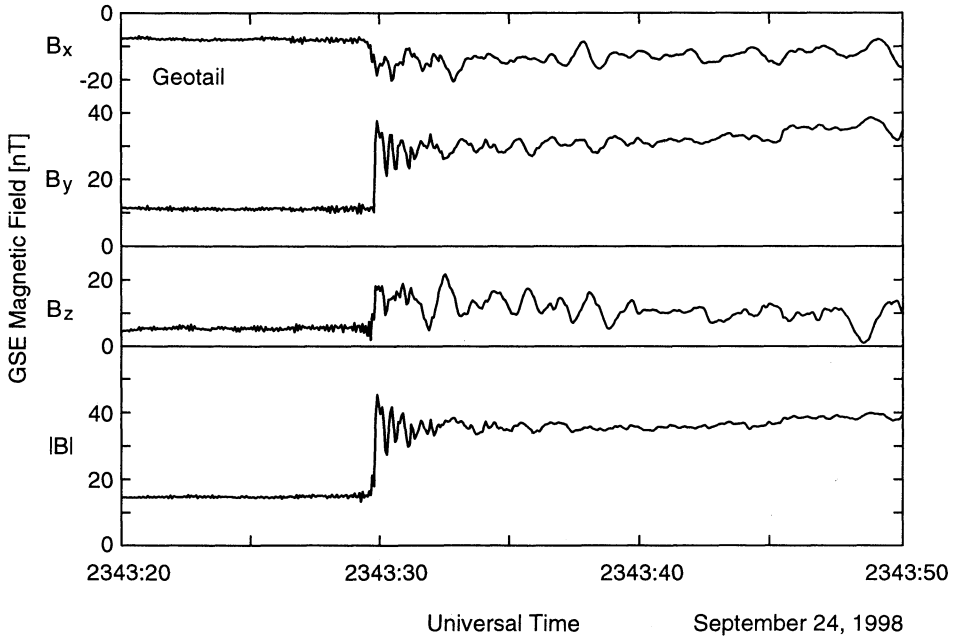

Figure 5. Magnetic field measured by Geotail across the interplanetary shock in GSE coordinates.

Table 2. Accuracies Required for a Maximum 1° Uncertainty in the Shock Orientation

Spacecraft	ΔT, s	ΔX, R_E	ΔY, R_E	ΔZ, R_E
ACE	9	1.1	3.8	2.3
Wind	7	0.9	3.0	1.8
Geotail	4	0.5	1.7	1.0
IMP 8	4	0.5	1.7	1.0

simulation box of global magnetosphere models. This allows an important cross check on calculations that use the shock velocity and orientation derived from the upstream measurements.

3. Shock Normal Determination

Shock normals can be determined by several different methods, either from observations at a single spacecraft using the magnetic field, possibly accompanied with solar wind data, or from multiple spacecraft again with observations of the magnetic field and possibly the plasma. These techniques are generally based on the relationship between the shock normal and a change in a parameter across the shock while some, such as the technique of *Vinas and Scudder* [1986], use the full set of Rankine-Hugoniot equations. To construct a shock normal formula based solely on the magnetic field, we note that the zero divergence of the magnetic requires that the change in the vector field is perpendicular to the shock normal. Further, the Rankine-Hugoniot relations show that the upstream and downstream magnetic fields are in the same plane as the shock normal so that the cross product of these two vectors is orthogonal to the shock normal. Thus the product of the difference field and the cross product of the upstream and downstream fields is along the shock normal [*Colburn and Sonett*, 1966]. This leads to the popular coplanarity normal whose formula is

$$\mathbf{n} \parallel (\mathbf{B}^u - \mathbf{B}^d) \times (\mathbf{B}^u \times \mathbf{B}^d). \tag{1}$$

This relationship is true outside the region of the shock potential drop [*Holzer et al.*, 1972]. In the shock layer itself a noncoplanar component of the magnetic field is observed that allows the electrons that are magnetized to cross the shock front and experience less of a potential drop than the ion [*Goodrich and Scudder*, 1984; *Jones and Ellison*, 1987; *Thomsen et al.*, 1987]. Thus care must be exercised to avoid including measurements within the shock layer in this calculation. The change in bulk velocity of the plasma across the shock is also coplanar with the shock normal and the upstream and downstream magnetic fields. By combining the cross product of either the upstream and downstream fields with the vector velocity change and with the change in the vector magnetic field, one obtains the mixed mode shock normal velocity [*Abraham-Shrauner,* 1972; *Abraham-Shrauner and Yun,* 1976].

$$\mathbf{n} \parallel (\mathbf{B}^u - \mathbf{B}^d) \times ((\mathbf{V}^u - \mathbf{V}^d) \times \mathbf{B}^u) \tag{2a}$$

$$\mathbf{n} \parallel (\mathbf{B}^u - \mathbf{B}^d) \times ((\mathbf{V}^u - \mathbf{V}^d) \times \mathbf{B}^d). \tag{2b}$$

We now have three equations that each determine the shock normal from a different set of measurements at a single location. We can combine the constraints that went into these three equations and incorporate measurements at different locations, labeled 1, 2 etc., using a matrix formalism.

$$\begin{bmatrix} \mathbf{B}_1^u - \mathbf{B}_1^d \\ \mathbf{B}_2^u - \mathbf{B}_2^d \\ \vdots \\ \mathbf{B}_1^u - \mathbf{B}_1^d \\ \mathbf{B}_2^u - \mathbf{B}_2^d \\ \vdots \\ (\mathbf{B}_1^u \times \Delta\mathbf{V}_1) \\ (\mathbf{B}_2^u \times \Delta\mathbf{V}_2) \\ \vdots \\ (\mathbf{B}_1^d \times \Delta\mathbf{V}_1) \\ (\mathbf{B}_2^d \times \Delta\mathbf{V}_2 \end{bmatrix} \bullet \begin{bmatrix} N_x \\ N_y \\ N_z \end{bmatrix} = 0. \tag{3}$$

This equation can be solved for the normal but does not return the shock speed. The shock speed may be determined from the conservation of mass that provides the shock speed in the frame in which the observations were obtained:

$$V_{sh} = \left(\frac{\rho^u \mathbf{V}^u - \rho^d \mathbf{V}^d}{\rho^u - \rho^d} \right) \bullet \mathbf{n}. \tag{4a}$$

We note that the shock speed is measured along the shock normal. A planar shock has only a component of velocity in this direction so that V_{sh} will appear here without a subscript denoting direction.

This approach can be used for any conserved quantity across the shock, not just the mass flux. Thus we can use the conservation of the tangential electric field, and write in the lmn shock frame with n along the shock normal and l along the projection of the upstream field on the shock plane:

$$V_{sh} = \left\{ \frac{B_l^u V_n^u - B_l^d V_n^d}{B_l^u - B_l^d} \right\} - \left\{ \frac{B_n V_l^u - B_n V_l^d}{B_l^u - B_l^d} \right\}. \tag{4b}$$

This expression avoids reliance on the density measure that depends on the plasma detector observing the entire distribution

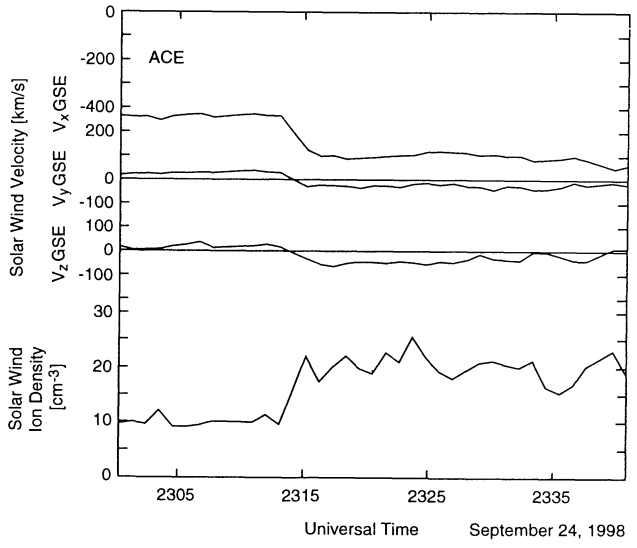

Figure 6. Solar wind velocity and density measured by the ACE spacecraft across the interplanetary shock.

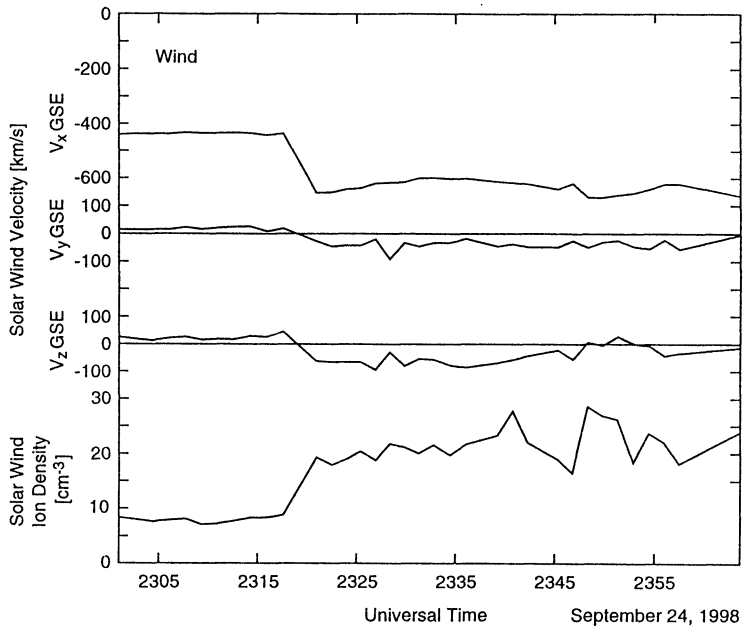

Figure 7. Solar wind velocity and density measured by the Wind spacecraft across the interplanetary shock.

in plasmas that may be quite different upstream and down. The accuracy of B_l and B_n depend on the accuracy with which the normal has been determined, whereas the scalar ρ has no such dependence on **n**. Thus the relative accuracy of (4a) and (4b) are to be determined.

Another way to obtain the shock velocity is to use the timing at multiple spacecraft [*Russell et al.*, 1983a]. This requires knowledge of the separation vectors between spacecraft $\Delta\mathbf{x}$ and the time for the shock to move from one to the other. It also assumes that the shock is planar in the region enclosed by the four spacecraft. This is a reasonable assumption for a structure whose radius of curvature is close to 1 AU, although it might have some level of rippling on its surface. If we designate one site to be location zero and reference the others to it, then

$$\begin{pmatrix} \Delta\mathbf{x}_{10} \\ \Delta\mathbf{x}_{20} \\ \Delta\mathbf{x}_{30} \end{pmatrix} \bullet \begin{pmatrix} n_x \\ n_y \\ n_z \end{pmatrix} = V_{\mathrm{sh}} \begin{pmatrix} \Delta t_{10} \\ \Delta t_{20} \\ \Delta t_{30} \end{pmatrix}. \tag{5}$$

This can be solved for V_{sh} and n without reference to any other measurements if there are observations of the timing of the encounter with the shock at four or more locations. For possibly even greater accuracy, both the time deltas and the plasma and field data can be combined into one overdetermined solution. In the section below we do this, as well as examine local solutions at each spacecraft.

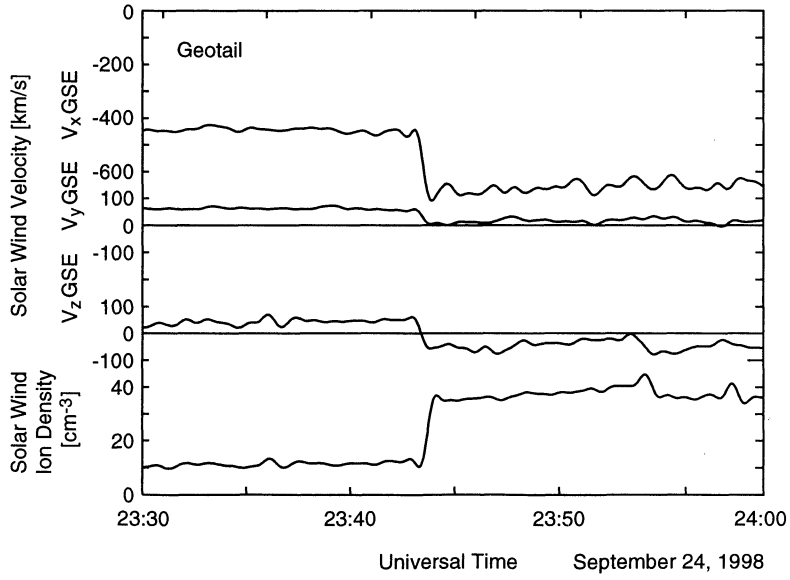

Figure 8. Solar wind velocity and density measured by the Geotail spacecraft across the interplanetary shock.

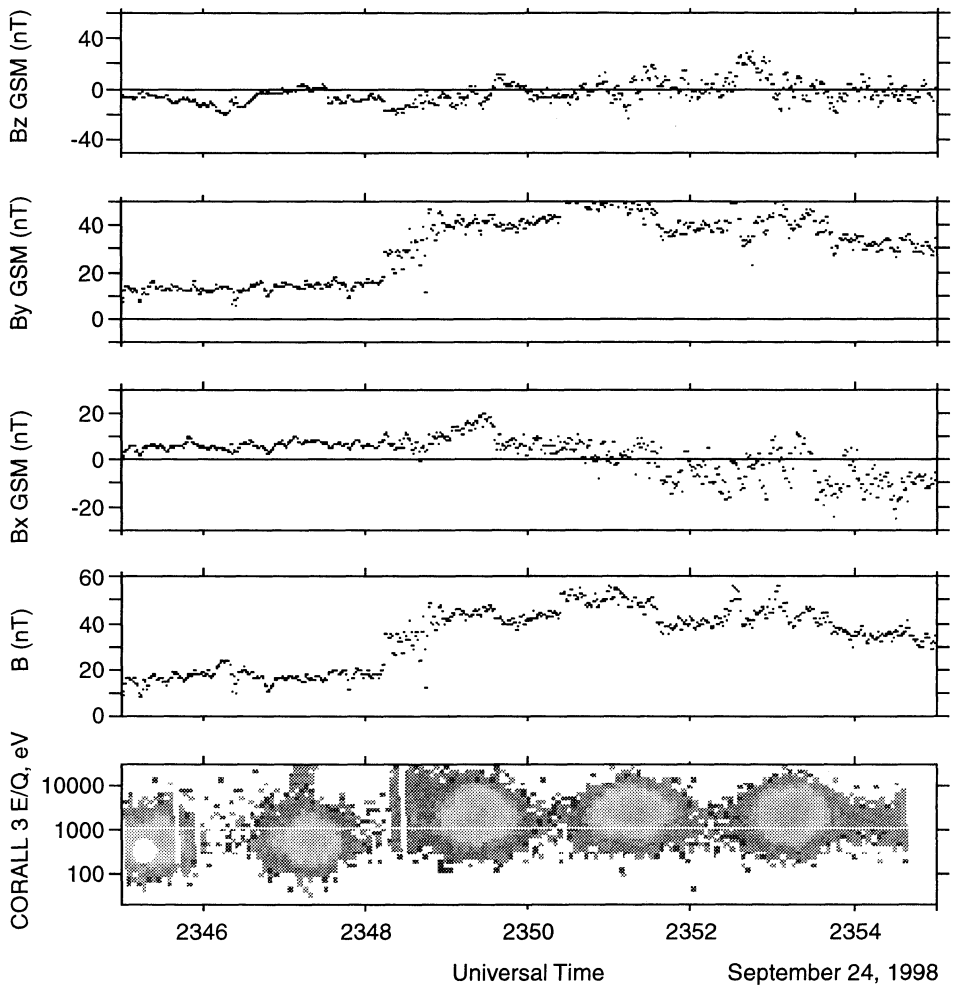

Figure 9. Magnetic field and plasma ion measurements by Interball on September 24, 1998, in the magnetosheath at the time of the shock passage.

4. Shock Normal Solutions

On September 24, 1998, when the interplanetary shock arrived, we have both magnetic field and three-dimensional plasma flow data at multiple locations in the solar wind. These data allow us not only to determine a precise shock orientation (our ultimate goal) but also to explore the relative accuracy of the various techniques used to measure shock orientations. Further, these data allow us to test the assumption of time stationarity of the shock orientation and speed by comparing our local solution with global solutions averaged over all the data.

4.1. Magnetic Coplanarity Normals

Suitable magnetic measurements are available upstream and downstream of each of three shock crossings: ACE, Wind, and Geotail. Table 3 lists the upstream and downstream magnetic vectors and the resultant normal at each location.

We note that since $\mathbf{B}^u$ and $\mathbf{B}^d$ are both in the coplanarity plane so is their difference, $\mathbf{B}^u$-$\mathbf{B}^d$, and their cross product is at right angles to the coplanarity plane, at right angles to $\mathbf{B}^u$-$\mathbf{B}^d$, (and of course to $\mathbf{n}$). Thus the only important angle, in determining the accuracy of the triple cross product defining the normal direction, is the angle between $\mathbf{B}^u$ and $\mathbf{B}^d$. This angle α is given in the last column of Table 3. We note that the three normals do differ from one another, but we do not know at this stage whether this difference is due to the inherent limitations of the method or represents a real difference in the shock orientation at each point.

4.2. Mixed Mode Normals

Three-dimensional velocity measurements are available from ACE, Wind, and Geotail. This computation can be performed with either the upstream or downstream magnetic field. Table 4 gives the velocity measurements upstream and downstream from the shock. The upstream and downstream fields are given in Table 3. The angle that determines the accuracy of this calculation is the angle between $\Delta\mathbf{V}$ and $\mathbf{B}$ for the same reason discussed in the case above. Again this angle is given in the last column of Table 4. We note that there is very little difference between the normal using the upstream or downstream magnetic field value.

4.3. Divergence-of-B-Only Normals

The above normals were derived for individual shock crossings. These single-site solutions suggest that the normals are similar at each location and possibly not significantly different from each other. Thus it is reasonable to combine measurements from different sites in a single solution. The divergence-free

Table 3. Single-Site Magnetic Coplanarity Normals

Spacecraft	$\mathbf{B}^u$, nT	$\mathbf{B}^d$, nT	n	α, deg
ACE	-6.90, 11.45, 4.11	-11.92, 31.12, 11.37	-0.972, -0.210, -0.104	9.8
Wind	-8.90, 9.65, -1.12	-11.72, 27.50, -3.78	-0.987, -0.146, 0.065	19.6
Geotail	-7.78, 11.26, 5.14	-14.65, 29.62, 13.42	-0.946, -0.301, -0.117	7.9

nature of the magnetic field means for the thin shock that the difference between the upstream and downstream fields lies in the shock plane. If we make two such measurements at different sites and if those field differences are at a significant angle to one another, then an estimate of the normal can be obtained. Table 5 shows the results of this calculation. The last column gives the angle α between the vector differences at the two spacecraft.

The ACE-Wind and Wind-Geotail pairs give similar normals to each other and to the previous results, but the ACE-Geotail result is significantly different. The angle α in the last column of Table 5 suggests why. The magnetic fields at ACE and Geotail are similar both upstream and down so that the changes in field at the two spacecraft are nearly parallel. The fields at Wind are different from those at the other two spacecraft and give a more accurate cross product with observations at the other two spacecraft. Thus the two normals that involve comparison of the field difference at Wind with that at the other two spacecraft are most accurate.

4.4. Magnetic Coplanarity - Only Normals

The usual coplanarity normal, discussed in section 4.1, uses both the divergence of **B** and the coplanarity theorem. As in section 4.3, we can use the cross product of the upstream and downstream fields at two sites to calculate a normal if these directions perpendicular to the coplanarity plane are sufficiently different at the two sites. This solution may be thought to be less accurate than the divergence of **B** normals because it is based on a less fundamental theorem than $\nabla \bullet \mathbf{B} = 0$ but also because within the shock there can be noncoplanar magnetic fields. Operationally, these may be difficult to avoid in calculating the average upstream and downstream fields. Table 6 lists these normals. All calculations seem to be significantly different than our earlier calculations and with each other.

4.5. Velocity Jump - Only Normals

The cross product between the upstream or downstream field and the velocity jump across the shock also gives a vector in the shock plane that can be compared at the two shocks. For the reasons stated above that this law is not as fundamental as the $\nabla \bullet \mathbf{B}$ relation and that the velocity is a less precise measurement than that of the magnetic field, we might expect this solution to be the least precise so far. Again since we can make the calculation using either the upstream or downstream vector field, we get a second set of normals, but these pairs of normals are almost identical. Table 7 gives these normals. We do not list normals derived from an upstream field at one site and a downstream field at another. These normals were similar to those listed in Table 7.

This calculation also appears to have a lot of scatter, but the ACE-Wind and Wind-Geotail normals are very similar in direction to the tight cluster of values we obtained with both single-site mixed-mode and magnetic coplanarity calculations in Tables 3 and 4.

4.5. Timing - Only Normals

Since we have the time of arrival of the shock at four quite distinct locations as given in Table 1 and since we can time the arrival and measure the location of the spacecraft to approximately the accuracies given in Table 2, we would expect this normal to be the most accurate of all. Again we recall that implicit in this solution is the assumption that the shock is planar in the region of the four spacecraft. Solving for the shock orientation and velocity with the positions given in Table 1, except for Interball, we obtain a normal of (-0.869, -0.255, -0.425) and speed of 695.7 km/s along that normal. This normal appears to be significantly different than the normals obtained at each site by magnetic coplanarity and the velocity jump crossed into the field values which normals agreed well with each other. Thus it is difficult to invoke shock curvature as a source of error. The most plausible source of error is either the timing at IMP 8 or its location. We return to this point in the discussion section after we calculate our best normal and shock speed independent of the IMP 8 data.

5. Discussion

In this paper we have examined a variety of techniques for determining the orientation of the shock normal. These several techniques have returned different solutions as displayed in Figure 10. It is now time to try to define a best fit result from these various solutions. First, as discussed above, we drop from consideration the four spacecraft-timing results from these various solutions. As most clearly seen in the bottom panel of Figure 10 it is inconsistent with the results from the other techniques. The reason for this inconsistency appears to be an error in either the timing or location of the IMP 8 spacecraft. The observations at ACE, Wind, and Geotail give six values of the shock velocity from mass and from electric field conservation using (4a) and (4b). These six estimates, none of which is dependent on IMP 8, give a shock speed of 762 ± 12 km/s. Our

Table 4. Single-Site Mixed Mode Coplanarity Normals

Spacecraft	Field	$\mathbf{V}^u$, km/s	$\mathbf{V}^d$, km/s	n	α, deg
ACE	upstream	-431.7, 63.3, 20.1	-603.9, 2.5, -50.5	-0.948, -0.135, -0.289	86
	downstream			-0.946, -0.133, -0.295	85
Wind	upstream	-438.4, 17.4, 27.5	-646.7, -44.4, -65.9	-0.900, -0.200, -0.388	64
	downstream			-0.895, -0.201, -0.398	81
Geotail	upstream	-453.7, 56.5, 52.1	-672.1, 7.7, -48.5	-0.906, -0.163, -0.391	80
	downstream			-0.906, -0.162, -0.392	87

Table 5. Multisite Divergence of **B** Normals

Satellite Pair	n	α, deg.
ACE-Wind	-0.967, -0.180, -0.181	28.5
ACE-Geotail	-0.562, 0.156, -0.812	6.6
Wind-Geotail	-0.923, -0.195, -0.332	33.3

"best fit" solution discussed below that includes no IMP 8 data returns a speed of 769 ± 2.5 km/s, well within the calculated probable error of the mean. Moreover, in Figure 10 we see no evidence for the shock normal to vary from one spacecraft to the next within the errors evident in these analyses, and finally, as we show below, the timing of events seen in the magnetosphere and magnetosheath by GOES 10, Polar, and Interball are consistent with the prediction we get by dropping the IMP 8 timing constraint. Thus we use only data from ACE, Wind, and Geotail. We first combine (3) with the first two rows of (5) and use all the data in Tables 1, 3, and 4. Because of their much greater intrinsic accuracy, up to 1 part in 10,000, we weight the equations containing time and space differences 100 times more than the equations containing plasma and field data. Inverting this matrix we obtain the solution labeled case 1 in Table 8. The magnetic field at ACE and Geotail, adjacent spacecraft in projection in Figure 2, is very similar. Thus the field changes at Geotail do not add much accuracy to the solution. If we drop the Geotail field values we get the value labeled case 2. The velocity data, as discussed above and as can be seen from the velocity coplanarity normals in Figure 10 are less accurate than the magnetic field data. If we remove them from the solution we get case 3. These three solutions are essentially identical. If we average them we get the bottom entry in Table 8. This is drawn as the horizontal line in Figure 10. As a consistency check, if we use this shock normal and its speed to derive the travel time from ACE to Geotail, we obtain a travel time that is too long by 1.2 s. For ACE and Wind we obtain a value that is too long by 0.3 s.

Extrapolated from Geotail using the best fit shock velocity, the interplanetary shock is expected to reach the terrestrial bow shock (14, 0, 0) R_E GSE at 2343:49 UT with an estimated error of <1 s. The expected time of arrival at the magnetopause at 10 R_E using the MHD model [*Raeder*, 1999] is 2344:19 UT. The arrival time of the compression due to the shock at GOES 10 at 1444 LT is predicted to be 2344:30. It is observed 25 s later at 2344:55. This late arrival could be due to the presence of ionospherically derived plasma that slows wave propagation and that is not present in the MHD simulation which derives its plasma from the solar wind. The arrival time at Polar above the polar cap at (-2.40, 2.72, 8.14) R_E GSM is predicted to occur at 2345:09 and is observed at 2345:10 UT, 1s later. The arrival of the shock at Interball in the post-terminator magnetosheath is predicted to be 2348:27 and is observed at 2348:15 UT, 12 s early.

As a final test we note that the Polar ultra violet imager (UVI) was viewing the northern polar cap with a cadence of one image per 37 s when this shock struck the magnetosphere (X. Y. Zhou and B. T. Tsurutani, Substorms, pseudobreakups, and quiescent events caused by interplanetary shocks, submitted to *Journal of Geophysical Research*, 2000). Six dayside views of the UVI data are shown in Figure 11. The brightening of the dayside aurora clearly occurs between the frames at 2344:07 and the frame at 2344:44, and the symmetry of the brightening suggests that the shock hit the magnetopause near noon, that is the x component of the shock normal was large. Again these observations are totally consistent with our calculated arrival times and shock normal orientation.

Our tests indicate that our best fit normal direction and speed are accurate, so it is appropriate to use these values to determine how accurate are our individual measurements of the normal. In Figure 12 we take the individual solutions and compare them with our best fit solution as a function of the angle between the vectors in the cross product. Despite their small cross-product angles, the magnetic coplanarity solutions are clearly the best, about 5° from

Table 6. Multisite Coplanarity-Only Normals

Spacecraft Pair	n	α, deg.
ACE-Wind	-0.991, 0.130, 0.023	29.7
ACE-Geotail	-0.824, -0.523, -0.218	4.1
Wind-Geotail	-0.998, 0.043, 0.036	32.8

Table 7. Multisite Velocity Jump-Only Normals

Spacecraft Pair	Field Used	Normal	α, deg.
ACE-Wind	upstream	-0.802, -0.438, -0.406	15.4
	downstream	-0.841, -0.381, -0.383	23.5
ACE-Geotail	upstream	-0.911, 0.412, -0.006	7.6
	downstream	-0.895, 0.445, -0.016	7.2
Wind-Geotail	upstream	-0.914, -0.143, -0.380	20.6
	downstream	-0.900, -0.176, -0.399	28.3

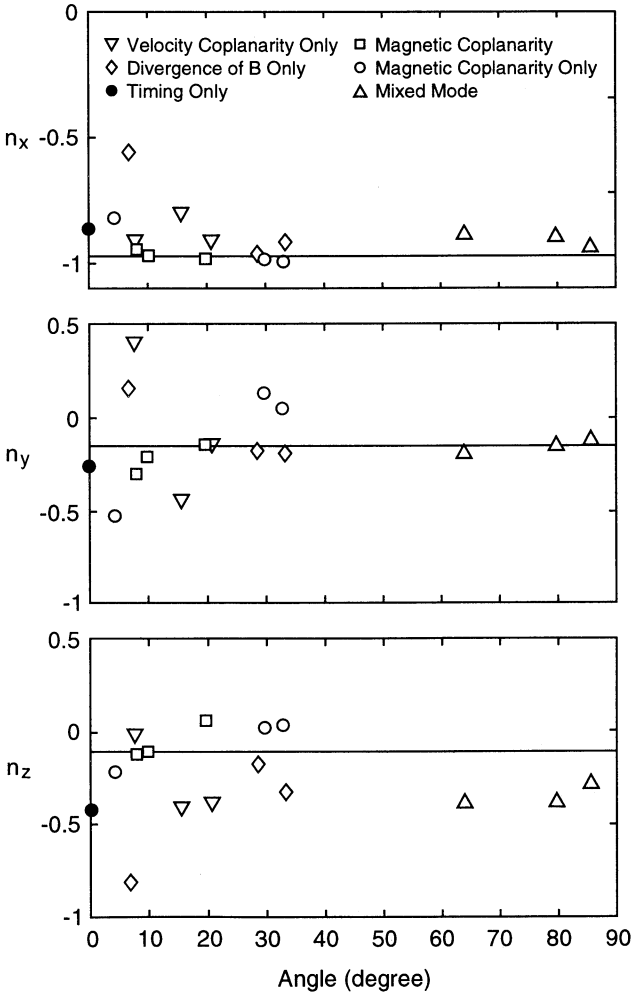

Figure 10. The components of the normal to the shock derived by each of our techniques as a function of the angle between the cross product vectors.

Table 8. Overdetermined Normals

	Normal	Speed, km/s
Case 1	-0.971 -0.175 -0.165	764
Case 2	-0.984 -0.152 -0.097	771
Case 3	-0.987 -0.144 -0.072	772
Average	-0.981 -0.157 -0.112	769 ± 2.5

Table 9. Wave Speeds and Mach Number

Satellite	V_A, km/s	C_s, km/s	V'', km/s	θ_{BN}, deg.	Mach Number
ACE	97	61	437	71.2	2.9
Wind	101	58	440	56.1	2.9
Geotail	87	59	460	68.8	3.0

the best fit. One of the reasons for the accuracy of this technique is that we are using very high resolution magnetic field data on shocks whose ramp is traversed rapidly and whose wave structure has limited upstream and downstream extent. In theory the technique relies on simultaneous upstream and downstream observations. In practice we take data upstream and down at different times. The closer these observations are to being simultaneous, the less is the chance that the upstream conditions appropriate to the downstream will not be different than those measured.

As a group the mixed mode normals are the next best, about 15° from the best fit. The divergence-of-B and the magnetic-coplanarity-only normals are next most accurate. If we ignore values with small critical angles α, the divergence-of-B-only normals are almost as accurate as the single-site magnetic coplanarity normals. The multisite velocity-jump normals have a typical error of about 25°. Part of the error in these normals is that for one pair of spacecraft the vector differences are small and the cross product is not well defined because the critical angle α is small. We note that we can calculate the shock speed from (4a), if we know the shock normal. Doing this for ACE, Wind, and Geotail using the single-site magnetic coplanarity normal, we obtain speeds of 736, 782, and 770 km/s, respectively, with an average and probable error of the mean of 763 ±14 km/s. We emphasize that none of the solar wind parameters used in this paper were derived from the key parameter data, but rather were obtained from the most refined data processing algorithms available at this time. Had we not used these more accurate values, there would have been a greater dispersion in the results obtained.

We can also perform this calculation using the tangential electric field with (4b) and the magnetic coplanarity normal from which we obtain speeds of 716, 772, and 797 km/s for ACE, Wind, and Geotail and an average of 762 ± 24 km/s. Both conservation estimates of the speed are similar and agree with our best fit shock speed of 769 ± 2.5 km/s well within their estimated errors, increasing our confidence in our assumption of the constancy of the shock speed and orientation in the volume bounded by ACE, Wind, and Geotail.

We can do one last accuracy check on our derivations by examining if the shock jumps that we see are in accord with the shock's Mach number. Table 9 gives the Alfven speed, the sound speed, the upstream solar wind velocity, the angle between the shock normal and the upstream magnetic field, as well as the desired Mach number using our optimum shock solution.

We can in turn use these Mach numbers to predict the downstream values from the upstream values according to the Rankine-Hugoniot conditions using $\gamma = 5/3$ that has previously been found to be appropriate for interplanetary shocks [*Russell et al.,* 1983b]. Table 10 shows the predicted values for the downstream density and magnetic field, for polytropic indices γ of 1.67 and 2. The former value is expected for a monatomic gas with three degrees of freedom, and the latter with two degrees of freedom. Here the values for $\gamma = 2$ are much closer to those observed than for $\gamma = 5/3$. Thus it appears that a collisionless shock can exhibit a polytropic index of 1.67 or 2. This dichotomy has also been observed in nonshocked situations at fast-slow stream boundaries [*Newbury et al.,* 1997].

None of the results discussed herein have used the IMP 8 data because the use of the IMP 8 location and timing gave values that

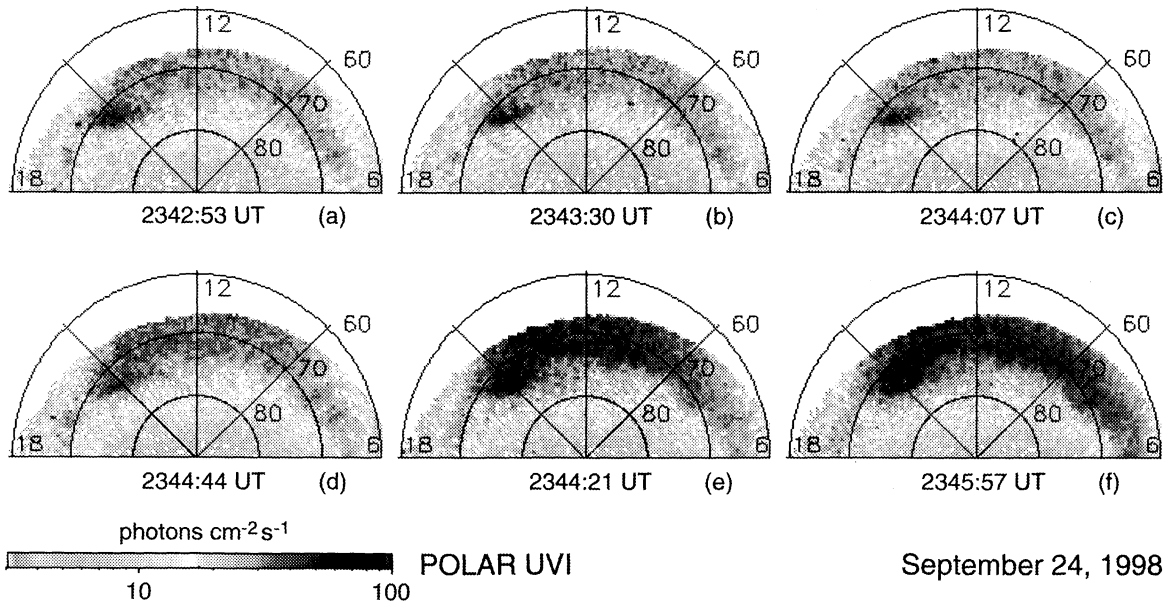

Figure 11. Six views of the dayside aurora as seen by the UVI images on Polar when the sudden impulse occurred.

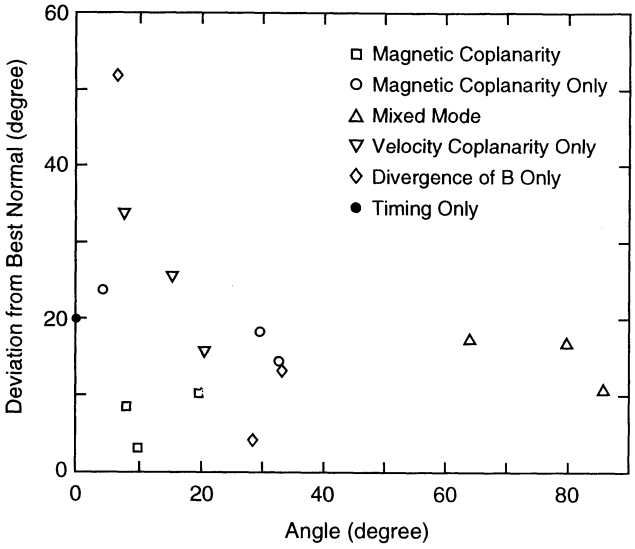

Figure 12. The angular deviation between our best fit normal and the normals derived from each of our techniques versus the angle between each of the cross-product vectors.

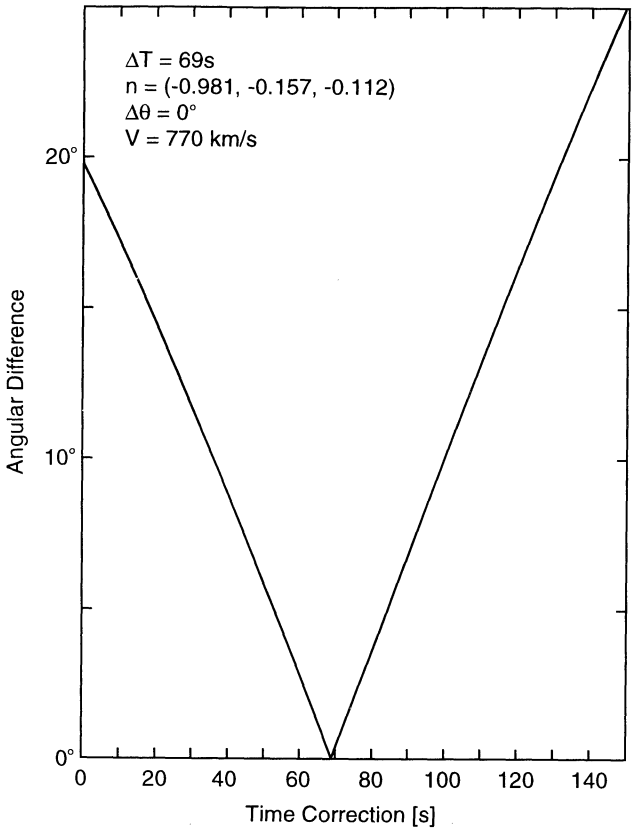

Figure 13. The angular difference between the four-spacecraft solution using IMP arrival data and the best fit normal as a function of the correction factor that is subtracted from the IMP 8 times. The "error" drops to 0° for a 69 s correction.

were quite inconsistent with other techniques. Moreover, as we have shown, our best fit solution is consistent with the time of arrival of the shock at the Earth as judged by observations at GOES 10, and both in situ and remote sensing data from Polar. It is instructive to determine what correction would bring IMP 8 into alignment with the other measurements. This exercise is carried out in Figure 13 that shows the angle between the four-spacecraft solution that includes IMP 8 location and timing and the best fit solution from the full suite of measurements from the other three spacecraft including their relative timing. The abscissa is the correction applied to the IMP 8 data in successive calculations of the four-spacecraft solution. When the IMP 8 data are corrected by subtracting 69 s, the angular error drops from 20° to 0° and the velocity increases from 696 to 770 km/s. This remarkable result brings the four-spacecraft solution into precise agreement with our best normal and velocity derived from the plasma and magnetometer data. Thus we cannot escape suggesting that an error has crept into the timing of the IMP 8 data system, with a magnitude of about 69 s. This error could be associated with the installation of the new ground systems for the receipt of data or may be a problem with the tagging of the magnetometer data only. The IMP project is investigating these possibilities, but at this writing we have not determined the source of the problem.

6. Conclusions

In summary, we would have expected a priori that the normal derived solely from timing and spacecraft locations to be the most accurate, but this appears not to be. The timing data and plasma data can be made consistent if we adjust the IMP 8 clock by 69 s. This also brings the extrapolated time of arrival of the shock in line with that observed within the magnetosphere. The single-site magnetic-coplanarity normals appear to be quite accurate. The mixed-mode coplanarity techniques at a single site were next most accurate. Techniques that involved cross products of data from different sites were less precise but still were moderately accurate unless the angles between vectors were at small angles to each other. The best solution was obtained when an overdetermined solution was attempted with all of the constraints or a large subset of them and the equations based on time and location were more heavily weighted. In calculating this overdetermined solution we have treated the shock surface as flat over the region enclosed by the spacecraft. There is nothing we have found that is inconsistent with this hypothesis, but certainly fluctuations in the normal direction of up to 5° are allowed by the coplanarity normal scatter. We also find that the polytropic index that best predicts the observed downstream values is very close to 2 for this shock and not 5/3 as seen for other shocks. In conclusion, the multiple observations available on September 24, 1998, have enabled us to determine a reliable shock speed

Table 10. Comparison of Predicted and Observed Downstream States

	Density, cm^{-3}			Magnetic Field, nT		
Satellite	Predicted (γ=1.67)	Predicted (γ=2)	Observed	Predicted (γ=1.67)	Predicted (γ=2)	Observed
ACE	27.7	23.7	22.5	38.3	32.7	35.2
Wind	23.4	19.9	20.2	34.2	29.1	30.1
Geotail	39.0	33.1	37.8	40.2	34.1	35.7

orientation and arrival at Earth. Additionally, we have been able to assess the relative accuracy of different techniques and to propose a reason for the one outlier in our statistics.

Acknowledgments. We wish to gratefully acknowledge S. Romanov for providing the Interball magnetometer data shown in Figure 9 and M. R. Aellig for providing the data shown in Figure 7. We are also grateful for providing the data shown in Figure 7 to J. King and W. Mish of GSFC for many useful discussions of the IMP mission and J. K. Chao for useful discussions on the formulas for determining shock speed. This research was supported at UCLA by the National Aeronautics and Space Administration under research grant NAG5-7721 at the Space Research Institute in Moscow by INTAS grant N97-1612. Support for ACE analysis at Bartol Research Institute by CIT subcontract PC251439 under NASA grant NAG5-6912.

Hiroshi Matsumoto thanks the referees for their assistance in evaluating this paper.

References

Abraham-Shrauner, B., Determination of magnetohydrodynamic shock normals, *J. Geophys. Res.*, *77*, 736-739, 1972.

Abraham-Shrauner, B., and S. H. Yun, Interplanetary shocks seen by Ames plasma probe on Pioneer 6 and 7, *J. Geophys. Res.*, *81*, 2097-2102, 1976.

Chi, P. J., C. T. Russell, S. Musman, W. K. Peterson, G. Le, V. Angelopoulos, G. D. Reeves, M. B. Moldwin, and F. K. Chun, Plasmaspheric depletion and refilling associated with the September 25, 1998 magnetic storm observed by ground magnetometers at L=2, *Geophys. Res. Lett.*, 27, 633-636, 2000.

Colburn, D. S., and C. P. Sonett, Discontinuities in the solar wind, *Space Sci. Rev.*, *5*, 439-506, 1966.

Goodrich, C. C., and J. D. Scudder, The adiabatic energy change of plasma electrons and the frame dependence of the cross-shock potential at collisionless magnetosonic shock waves, *J. Geophys. Res.*, *89*, 6654-6662, 1984.

Holzer, R. E., T. G. Northrop, J. V. Olson, and C. T. Russell, Study of waves in the Earth's bow shock, *J. Geophys. Res.*, *77*, 2264-2273, 1972.

Jones, F. C., and D. C. Ellison, Noncoplanar magnetic fields, shock potentials, and ion deflection, *J. Geophys. Res.*, 92, 11,205-11,207, 1987.

Klimov, S., et al., ASPI experiment: Measurements of fields and waves on board the INTERBALL-1 spacecraft, *Ann. Geophys.*, *15*, 514-527, 1997.

Kokubun, S., T. Yamamoto, M. H. Acuna, K. Hayashi, K. Shiokawa, and H. Kawano, The Geotail magnetic field experiment, *J. Geomagn. Geoelectr.*, *46*, 7-21, 1994.

Lepping, R. P., et al., The Wind magnetic field investigation, *Space Sci. Rev.*, *71*, 207-229, 1995.

McComas, D. J., S. J. Bame, P. Barker, W. C. Feldman, J. L. Phillips, P. Riley, and J. W. Griffee, Solar wind electron proton alpha monitor (SWEPAM) for the Advanced Composition Explorer, *Space Sci. Rev.*, *86*, 563-612, 1998.

Moore, T. E., W. K. Peterson, C. T. Russell, M. O. Chandler, M. R. Collier, H. L. Collin, P. D. Craven, R. Fitzenreiter, B. L. Giles, and C. J. Pollock, Ionospheric mass ejection in response to a CME, *Geophys. Res. Lett.*, *26*, 2339-2342, 1999.

Mukai, T., S. Machida, Y. Saito, M. Hirahara, T. Terasawa, N. Kaya, T. Obara, M. Ejiri and A. Nishida, Low energy particle experiment (LEP) onboard the Geotail satellite, *J. Geomagn. Geoelectr.*, *46*, 669-692, 1994.

Newbury, J. A., C. T. Russell, and G. M. Lindsay, Solar wind polytropic index in the vicinity of stream interactions, *Geophys. Res. Lett.*, *24*, 1431-1434, 1997.

Ogilvie, K. W., et al., SWE, a comprehensive plasma instrument for the Wind spacecraft, *Space Sci. Rev.*, *71*, 55-77, 1995.

Raeder, J., Modeling the magnetosphere for northward interplanetary magnetic field: Effects of electrical resistivity, *J. Geophys. Res.*, *104*, 17,357-17,367, 1999.

Russell, C. T., Results of the IASTP Program, *Adv. Space Res.*, *20*, 525-528, 1997.

Russell, C. T., and D. J. Southwood (eds.), *The IMS Source Book: Guide to the International Magnetospheric Study Data Analysis*, 304 pp. AGU, Washington, D. C., 1982.

Russell, C. T., M. M. Mellott, E. J. Smith, and J. H. King, Multiple spacecraft observations of interplanetary shocks: Four spacecraft determination of shock normals, *J. Geophys. Res.*, *88*, 4739-4748, 1983a.

Russell, C. T., J. T. Gosling, R. D. Zwickl, and E. J. Smith, Multiple spacecraft observations of interplanetary shocks: ISEE three-dimensional plasma measurements, *J. Geophys. Res.*, *88*, 9941-9947, 1983b.

Russell, C. T., X. W. Zhou, P. J. Chi, H. Kawano, T. E. Moore, W. K. Peterson, J. B. Cladis, and H. J. Singer, Sudden compression of the outer magnetosphere associated with an ionospheric mass ejection, *Geophys. Res. Lett.*, *26*, 2343-2346, 1999.

Smith, C. W., J. L. Heureux, N. F. Ness, M. H. Acuna, L. F. Burlaga, and J. Scheiffele, The ACE magnetic fields experiment, *Space Sci. Rev.*, *86*, 613-632, 1998.

Strangeway, R. J., C. T. Russell, C. W. Carlson, J. P. McFadden, R. E. Ergun, M. Temerin, D. M. Klumpar, W. K. Peterson, and T. E. Moore, Cusp field-aligned currents and ion outflows, *J. Geophys. Res.*, in press, 2000.

Thomsen, M. F., J. T. Gosling, S. J. Bame, K. B. Quest, D. Winske, W. A. Livesey, and C. T. Russell, On the noncoplanarity of the magnetic field within a fast collisionless shock, *J. Geophys. Res.*, *92*, 2305-2314, 1987.

Vinas, A. F., and J. D. Scudder, Fast and optimal solution to the Rankine-Hugoniot problem, *J. Geophys. Res.*, *91*, 39-58, 1986.

Yermolaev, Y. I., A. O. Fedorov, O. L. Vaisberg, V. M. Balebanov, Yu. A. Obod, R. Jimenez, J. Fleites, L. Llera, and A. N. Omelchenko, Ion distribution dynamics near the Earth's bow shock: First measurements with 2-D ion energy spectrometer CORALL on INTERBALL/ Tail Probe satellite, *Ann. Geophys.*, *15*, 533-541, 1997.

H. Kawano, Kyushu University 33, Higashi-Ku, Fukuoka 812-8581, Japan.

A. J. Lazarus, Massachusetts Institute of Technology, Rm 37-687, Cambridge, MA 02139 (ajl@space.mit.edu)

R. P. Lepping, K. W. Ogilvie, and A. Szabo, NASA Goddard Space Flight Center, MC 692, Greenbelt, MD 20771.

T. Mukai, Institute of Space and Astronautical Science, 311 Yoshinodai, Sagamihara Kanagawa 229, Japan.

J. Raeder, C. T. Russell, and Y. L. Wang, IGPP, University of California, 3845 Slichter Hall, 405 Hilgard Avenue, Los Angeles, CA 90095-1567 (ctrussell@igpp.ucla.edu)

S. Savin and Y. Yermolaev, Space Research Institute, Russian Academy of Sciences, 84/32 Profsojuznaya St., Moscow 117810, Russia.

C. W. Smith, Bartol Research Institute, University of Delaware, Newark, DE 19716.

R. L. Tokar, Los Alamos National Laboratory, Los Alamos, NM 87545.

B. T. Tsurutani and X.-Y. Zhou, Jet Propulsion Laboratory, 4800 Oak Grove Dr., MS-169-506, Pasadena, CA 91109.

(Received November 25, 1999; revised March 10, 2000;
accepted May 8, 2000.)